

## Numerical solution for MHD Flow of an Oldroyd-B fluid over a stretching sheet in the presence of thermophoresis with chemical reaction effects



Abdelmgid O. M. Sidahmed \*

Department of Mathematics, College of Science and Arts, King Abdulaziz University, Rabigh 21911, Saudi Arabia

### ARTICLE INFO

#### Article history:

Received 23 July 2023

Received in revised form

25 November 2023

Accepted 27 November 2023

#### Keywords:

MHD

Oldroyd-B fluid

Chemical reaction

SLM

### ABSTRACT

The magnetohydrodynamic flow of an Oldroyd-B fluid across a vertical stretching sheet through a porous medium is investigated. Using a similarity transformation, the boundary layer equations for momentum, thermal energy, and concentration can be simplified into a set of linked ordinary differential equations. The successive linearization method is then used to numerically solve the system of ordinary differential equations. Graphical and tabular representations of the physical parameter effects on velocity, temperature, concentration profiles, the local skin friction coefficient, and heat and mass transfer rates are provided. Deborah's number in terms of relaxation time has been reported to resist and slow down the motion of fluid particles at different time instants in terms of relaxation time. By raising Deborah's numbers in terms of relaxation time, the temperature profile rises. Additionally, excellent agreement was found after the current results were examined and contrasted with the published results.

© 2023 The Authors. Published by IASE. This is an open access article under the CC BY-NC-ND license (<http://creativecommons.org/licenses/by-nc-nd/4.0/>).

### 1. Introduction

Oldroyd-B fluids are non-Newtonian viscoelastic fluids classified as the rate type model. Models of the rate type are suitable for describing many of the non-Newtonian characteristics shown by polymeric materials, such as stress-relaxation, normal stress differences in simple shear flows and creep (Rubbab et al., 2009; Pires and Sequeira, 2011). Rheologists have recently paid a lot of attention to the Oldroyd-B model since it is primarily useful for simulating the behavior of diluted polymeric solutions. However, rate-type models are unable to accurately represent the complex rheological behavior of many real fluids, such as blood, where non-Newtonian viscosity factors play a significant role (Pires and Sequeira, 2011). Non-Newtonian fluids are used in a variety of fields of business and technology, including biomedicine, chemical engineering, the food and pharmaceutical industries, the manufacture of plastic sheets, and the extrusion of polymers via slit dies in the polymer sector, among others (Hayat et al., 2013; 2014; Azeem et al., 2014; Mabood et al., 2020; Shankaralingappa et al., 2021). An Oldroyd-B

model's boundary layer stagnation point flow toward a moving sheet was originally started by Sajid et al. (2010). They offered numerical answers for the velocity distribution of an infinite speed. Hayat et al. (2015) examined the mixed convection flow of an Oldroyd-B fluid over a radiative surface with the effects of double stratification and chemical reactions. Motsa et al. (2015) demonstrated numerically the three-dimensional flow of an Oldroyd-B fluid with time dependence. In the presence of homogeneous and heterogeneous processes, the Cattaneo-Christov heat flux was investigated by Hayat et al. (2016) in the context of the magnetohydrodynamic flow of an Oldroyd-B fluid. Similar studies can be found in the literature (Yasir et al., 2021; 2023; Yasir and Khan, 2023).

Gireesha et al. (2018) investigated the three-dimensional flow and nonlinear radiative heat transfer of an Oldroyd-B nanofluid flow over a stretching surface with the addition effects of a uniform heat source/sink and convective boundary conditions. They found that when the values of Deborah's numbers  $\beta_1$  were increased, temperature and concentration profiles increased.

Nonlinear equations can model many cosmic events that we encounter daily in science, physics, and geometry. Using approximate mathematical analytical techniques, some of these nonlinear equations can be solved, such as the Homotopy (HAM) analysis method introduced by Liao (2003) and the Adomian decomposition method (ADM)

\* Corresponding Author.

Email Address: [aoahmad2@kau.edu.sa](mailto:aoahmad2@kau.edu.sa)

<https://doi.org/10.21833/ijaas.2023.12.014>

Corresponding author's ORCID profile:

<https://orcid.org/0000-0002-1926-6162>

2313-626X/© 2023 The Authors. Published by IASE.

This is an open access article under the CC BY-NC-ND license

(<http://creativecommons.org/licenses/by-nc-nd/4.0/>)

(Makinde, 2008). Some of these equations can be resolved using traditional numerical techniques like the Keller box, Runge-Kutta, and finite difference methods. Recent investigations have demonstrated the effectiveness of a technique known as the successive linearization method (SLM). Numerous non-linear issues in science and engineering have been successfully solved using this approach. This technique has been used to convert the governing non-linear equations into a system of linear differential equations. To solve the higher-order deformation in linear differential equations, we used the Chebyshev pseudo-spectral approach. In comparison to other current semi-analytical approaches, such as the Adomian decomposition method, they demonstrated that the SLM swiftly converges to numerical values and is flexible, efficient, and accurate. The SLM technique can also be used to handle boundary value problems involving highly non-linear systems instead of more traditional numerical approaches (Makukula et al., 2010a; 2010b; Narayana and Sibanda, 2012; Shateyi and Motsa, 2010; Ahmed et al., 2015; Khidir, 2023; Daoud et al., 2021; Salah et al., 2019).

Chemical reactions are used in a variety of industrial processes, such as hot rolling, chemical plating of flat surfaces, polymer extrusion, and heat exchange (Reddy et al., 2021; Salah and Sidahmed, 2022). Seini and Makinde (2013) investigated how the MHD boundary layer moved across an exponentially stretched sheet when chemical reactions and radiation were present. By employing the Bvp4c method, Paul and Das (2023) studied a two-dimensional stable issue that integrates the magnetohydrodynamic effect with three separate flows of fluid from the boundary layer across an exponentially stretched sheet under the impact of thermal radiation and chemical reactions. There are some interesting contributions to chemical reactions in the literature (Khan et al., 2022; Salah, 2022; Sidahmed and Salah, 2022; Yasir and Khan, 2023).

The purpose of this study is to extend the results of Noor (2012) and Shateyi (2013), such as how the magnetohydrodynamic flow of an Oldroyd-B model affects across a vertical stretching sheet through a porous medium with chemical reaction.

An original study is currently being conducted on the MHD flow of an Oldroyd-B fluid over a stretching sheet when thermophoresis and chemical reaction effects are present. MHD is employed with the governing equations for the Oldroyd-B liquid. The numerical solution to the resulting nonlinear problem is computed using the SLM method. Embedded flow parameters are described and displayed using diagrams.

## 2. Mathematical formulation

### 2.1. Governing equations and boundary conditions

Here, we are interested in the steady two-dimensional laminar flow of an incompressible MHD

Oldroyd-B fluid through a flat sheet that lines up with the plane  $y = 0$ , stopping the flow at  $y > 0$ . Equal forces are applied to two opposed objects along the  $x$ -axis. As a result, the wall is stretched, and the origin is fixed. Along the sheet, there are variations in both the temperature distribution  $T_w(x)$  and the concentration distribution  $C_w(x)$ . While  $T_w > T_\infty$  and  $C_\infty$ , the fluid has a uniform ambient temperature  $T_\infty$  and concentration  $C_\infty$ . The continuity constitutive equation of the Oldroyd-B fluid and energy equation is given below under the constant and boundary layer assumptions (Cortell, 2006; Waqas et al., 2018; Ghadikolaei et al., 2018).

$$\frac{\partial u}{\partial x} + \frac{\partial v}{\partial y} = 0, \tag{1}$$

$$u \frac{\partial u}{\partial x} + v \frac{\partial u}{\partial y} + \beta \left( u^2 \frac{\partial^2 u}{\partial x^2} + v^2 \frac{\partial^2 u}{\partial y^2} + 2uv \frac{\partial^2 u}{\partial x \partial y} \right) = v \left[ \frac{\partial^2 u}{\partial y^2} + \Gamma \left( \frac{\partial}{\partial x} \left( u \frac{\partial^2 u}{\partial y^2} \right) + \frac{\partial u}{\partial y} \frac{\partial^2 v}{\partial y^2} + v \frac{\partial^3 u}{\partial y^3} \right) \right] - \frac{\sigma B_0^2}{\rho} \left( u + \beta v \frac{\partial u}{\partial y} \right) - \frac{v}{K} u + g\beta_T(T - T_\infty) + g\beta_C(C - C_\infty), \tag{2}$$

$$u \frac{\partial T}{\partial x} + v \frac{\partial T}{\partial y} - \frac{\sigma B_0^2}{\rho c_p} u^2 = \frac{\lambda_g}{\rho c_p} \frac{\partial^2 T}{\partial y^2} + \frac{\mu}{\rho c_p} \left( \frac{\partial u}{\partial y} \right)^2 - \frac{1}{\rho c_p} \frac{\partial q_r}{\partial y}, \tag{3}$$

$$u \frac{\partial C}{\partial x} + v \frac{\partial C}{\partial y} = D \frac{\partial^2 C}{\partial y^2} - \frac{\partial(V_T C)}{\partial y} - k_2 C. \tag{4}$$

With boundary conditions,

$$u(x, 0) = U_w(x) = ax, \quad v(x, 0) = 0, \tag{5}$$

$$T(x, 0) = T_\infty + bx, \quad C(x, 0) = C + cx, \tag{6}$$

$$u(x, \infty) = 0, \quad T(x, \infty) = T_\infty, \quad C(x, \infty) = C_\infty,$$

where,  $(u, v)$  are the components of velocity in  $(x, y)$  directions,  $\beta$  is the relaxation time,  $\nu \left( = \frac{\mu}{\rho} \right)$  is the kinematic viscosity,  $\mu$  is the dynamic viscosity,  $\Gamma$  is the retardation time,  $\rho$  is density of fluid,  $K$  is the permeability of the porous medium,  $\sigma$  is the electric conductivity,  $B_0$  is the uniform magnetic fluid,  $g$  is the gravitational acceleration,  $C$  is the fluid concentration,  $T$  is the fluid temperature,  $\beta_T$  is the coefficient of thermal expansion,  $\beta_C$  is the coefficient of concentration expansion,  $\lambda_g$  is the fluid thermal conductivity,  $c_p$  is the specific heat at constant pressure,  $q_r$  is the radiative heat flux,  $D$  is the molecular diffusivity of the species concentration,  $V_T$  is the thermophoretic velocity and  $K_2$  is the chemical reaction parameter. The radiative heat flux  $q_r$  can be written by Raptis (1998).

$$q_r = - \frac{4\sigma^* \partial T^4}{3K_s \partial y}. \tag{7}$$

The Rosseland mean absorption coefficient and the Stefan-Boltzman constant, respectively, are denoted by  $\sigma^*$  and  $K_s$ . Assuming that the temperature changes within the flow are negligibly small,  $T^4$  can be represented as a linear function of temperature.

$$T^4 \approx 4T_\infty^3 T - 3T_\infty^4. \tag{8}$$

When we apply Eqs. 7 and 8 to the final term in Eq. 3, we get:

$$\frac{\partial q_r}{\partial y} = \frac{16\sigma^* T_\infty^3}{3K_s} \frac{\partial^2 T}{\partial y^2} \tag{9}$$

Eq. 4 contains the thermophoretic velocity  $V_T$ , which is expressed as:

$$V_T = \frac{kv}{T_r} \frac{\partial T}{\partial y'} \tag{10}$$

where,  $k$  is the thermophoretic coefficient, having a range of values from 0.2 to 1.2, and  $T_r$  is the reference temperature. A thermophoretic parameter  $\tau$  is defined as:

$$\tau = -\frac{k(T_w - T_\infty)}{T_r} \tag{11}$$

**2.2. Similarity transformation**

The following non-dimensional variables (Cortell, 2006; Ghadikolaei et al., 2018) can be used to convert the governing Eqs. 2-4 into a set of nonlinear ordinary differential equations:

$$u = cx f'(\eta), v = -\sqrt{c\nu} f(\eta), \eta = \sqrt{\frac{c}{\nu}} y', \theta = \frac{T - T_\infty}{T_w - T_\infty}, \phi = \frac{C - C_\infty}{C_w - C_\infty} \tag{12}$$

The following set of non-linear ordinary differential equations is produced by applying Eq. 12 to the governing equations.

$$f'''' + (1 + M\beta_1)ff'' - f'^2 + \beta_1(2ff'f'' - f^2f''') + \beta_2(2f'f''' - f''^2 - ff^{iv}) - (M + \lambda)f' + \gamma[\theta + N\phi] = 0, \tag{13}$$

$$\left(1 + \frac{4}{3}R\right)\theta'' + Pr(f\theta' - f'\theta) + PrEc(Mf'^2 + f''^2) = 0, \tag{14}$$

$$\phi'' + Sc[f\phi' - f'\phi - \tau(\theta'\phi' + \theta''\phi)] - K_2\phi = 0. \tag{15}$$

where,  $\beta_1(= \beta c)$  and  $\beta_2(= c \Gamma)$  is relaxation and retardation times, respectively,  $M(= \sigma\beta_0^2/c\rho)$  is the Hartman number,  $\lambda(= \frac{\nu}{aK})$  is the porosity parameter,  $\gamma(= \frac{Gr_x}{Re_x^2})$  is the local buoyancy parameter,  $R = 4\sigma^*/K_s\lambda_g$  is the radiation parameter,  $Pr$  is the Prandtl number,  $Ec$  is the Eckert number,  $Sc$  is the Schmidt number and  $K_2$  is the chemical reaction. The boundary conditions are:

$$f(0) = 0, f'(0) = 1, \theta(0) = 1, \phi(0) = 1, \tag{16}$$

$$f' \rightarrow 0, \theta \rightarrow 0, \phi \rightarrow 0, \text{ as } \eta \rightarrow \infty. \tag{17}$$

$$r_{1,i-1} = \beta_2 \sum_{j=0}^{i-1} f_j \sum_{j=0}^{i-1} f_j^{iv} - \sum_{j=0}^{i-1} f_j''' - (1 + M\beta_1) \sum_{j=0}^{i-1} f_j \sum_{j=0}^{i-1} f_j'' + \beta_1 \sum_{j=0}^{i-1} f_j''' (\sum_{j=0}^{i-1} f_j)^2 - 2\beta_1 \sum_{j=0}^{i-1} f_j \sum_{j=0}^{i-1} f_j' \sum_{j=0}^{i-1} f_j'' -$$

$$2\beta_2 \sum_{j=0}^{i-1} f_j' \sum_{j=0}^{i-1} f_j''' + \beta_2 (\sum_{j=0}^{i-1} f_j'')^2 + (\sum_{j=0}^{i-1} f_j')^2 + (\lambda + M) \sum_{j=0}^{i-1} f_j' - \gamma \sum_{j=0}^{i-1} \theta_j - N\gamma \sum_{j=0}^{i-1} \phi_j,$$

$$r_{2,i-1} = -\left(1 + \frac{4}{3}R\right) \sum_{j=0}^{i-1} \theta_j'' - Pr \sum_{j=0}^{i-1} f_j \sum_{j=0}^{i-1} \theta_j' + Pr \sum_{j=0}^{i-1} \theta_j \sum_{j=0}^{i-1} f_j' - PrEc(\sum_{j=0}^{i-1} f_j'')^2 - (Pr)(Ec)(M)(\sum_{j=0}^{i-1} f_j')^2,$$

$$r_{3,i-1} = -\sum_{j=0}^{i-1} \phi_j'' - Sc \sum_{j=0}^{i-1} f_j \sum_{j=0}^{i-1} \phi_j' + Sc \tau \sum_{j=0}^{i-1} \phi_j' \sum_{j=0}^{i-1} \theta_j' + Sc \sum_{j=0}^{i-1} \phi_j \sum_{j=0}^{i-1} f_j' + Sc \tau \sum_{j=0}^{i-1} \phi_j \sum_{j=0}^{i-1} \theta_j'' + K_2 \sum_{j=0}^{i-1} \phi_j,$$

Using the Chebyshev collocation spectral method (Hussaini and Zang, 1987), the linearized system is solved, producing the following system of equations:

$$\begin{aligned} A_{11} f_i + A_{12} \theta_i + A_{13} \phi_i &= r_{1,i-1} \\ A_{21} f_i + A_{22} \theta_i + A_{23} \phi_i &= r_{2,i-1} \\ A_{31} f_i + A_{32} \theta_i + A_{33} \phi_i &= r_{3,i-1} \end{aligned} \tag{23}$$

**3. Numerical methods**

We employ SLM to solve the current problem numerically. The SLM works by iteratively converting the controlling nonlinear Eqs. 13-15 into a set of linear differential equations, which are then solved analytically or numerically.

The SLM technique presupposes that the solution of system of Eqs. 13-15 can be represented as (Salah et al., 2023; Ahmed et al., 2016; Salah and Elhafian, 2019):

$$f(\eta) = f_i(\eta) + \sum_{n=0}^{i-1} f_n(\eta), \theta(\eta) = \theta_i(\eta) + \sum_{n=0}^{i-1} \theta_n(\eta), \phi(\eta) = \phi_i(\eta) + \sum_{n=0}^{i-1} \phi_n(\eta). \tag{18}$$

Starting from an initial guess that is appropriate for  $f_0(\eta)$ ,  $\theta_0(\eta)$  and  $\phi_0(\eta)$  and satisfies the boundary conditions of Eq. 16 and Eq. 17, suitable functions are as follows.

$$f_0(\eta) = 1 - e^{-\eta}, \theta_0(\eta) = e^{-\eta}, \phi_0(\eta) = e^{-\eta}. \tag{19}$$

Substituting Eq. 18 into the controlling Eqs. 13-15 while neglecting the nonlinear factors in  $f_i(\eta)$ ,  $\theta_i(\eta)$  and  $\phi_i(\eta)$  and their derivatives yields:

$$\begin{aligned} &(-\beta_2 \sum_{j=0}^{i-1} f_j) f_i^{iv} + (1 - \beta_1 (\sum_{j=0}^{i-1} f_j)^2 + 2\beta_2 \sum_{j=0}^{i-1} f_j') f_i''' + \\ &((1 + M\beta_1) \sum_{j=0}^{i-1} f_j + 2\beta_1 \sum_{j=0}^{i-1} f_j \sum_{j=0}^{i-1} f_j' - \\ &2\beta_2 \sum_{j=0}^{i-1} f_j'') f_i'' + (2\beta_1 \sum_{j=0}^{i-1} f_j \sum_{j=0}^{i-1} f_j'' - 2 \sum_{j=0}^{i-1} f_j' + \\ &2\beta_2 \sum_{j=0}^{i-1} f_j'' - \lambda - M) f_i' + ((1 + M\beta_1) \sum_{j=0}^{i-1} f_j'' + \\ &2\beta_1 \sum_{j=0}^{i-1} f_j' \sum_{j=0}^{i-1} f_j'' - 2\beta_1 \sum_{j=0}^{i-1} f_j \sum_{j=0}^{i-1} f_j''' - \\ &\beta_2 \sum_{j=0}^{i-1} f_j^{iv}) f_i + \gamma \theta_i + N\gamma \phi_i = r_{1,i-1} \end{aligned} \tag{20}$$

$$\begin{aligned} &\left(1 + \frac{4}{3}R\right) \theta_i'' + Pr(\sum_{j=0}^{i-1} f_j) \theta_i' - Pr(\sum_{j=0}^{i-1} f_j') \theta_i + \\ &2 Pr Ec (\sum_{j=0}^{i-1} f_j'') f_i'' + (2MPrEc \sum_{j=0}^{i-1} f_j' - Pr \sum_{j=0}^{i-1} \theta_j) f_i' + \\ &Pr(\sum_{j=0}^{i-1} \theta_j') f_i = r_{2,i-1} \end{aligned} \tag{21}$$

$$\begin{aligned} &\phi_i'' + Sc(\sum_{j=0}^{i-1} f_j - \tau \sum_{j=0}^{i-1} \theta_j') \phi_i' + (K_2 - Sc \sum_{j=0}^{i-1} f_j' - \\ &Sc \tau \sum_{j=0}^{i-1} \theta_j'') \phi_i - Sc (\sum_{j=0}^{i-1} \phi_j) f_i' + Sc (\sum_{j=0}^{i-1} \phi_j') f_i - \\ &Sc \tau (\sum_{j=0}^{i-1} \phi_j) \theta_i'' - Sc \tau (\sum_{j=0}^{i-1} \phi_j) \theta_i' = r_{3,i-1} \end{aligned} \tag{22}$$

depending on the conditions at the boundary,

$$f_i(0) = f_i'(0) = f_i'(\infty) = 0, \theta_i(0) = \theta_i(\infty) = 0, \phi_i(0) = \phi_i(\infty) = 0.$$

where,

We can write the system in Eq. 23 as matrix equation:

$$A_{i-1} X_i = R_{i-1}, \tag{24}$$

where,

$$A_{i-1} = \begin{bmatrix} A_{11} & A_{12} & A_{13} \\ A_{21} & A_{22} & A_{23} \\ A_{31} & A_{32} & A_{33} \end{bmatrix}, X_i = \begin{bmatrix} f_i \\ \theta_i \\ \phi_i \end{bmatrix}, R_{i-1} = \begin{bmatrix} r_{1,i-1} \\ r_{2,i-1} \\ r_{3,i-1} \end{bmatrix}, \text{ and,}$$

$$\begin{aligned} A_{11} &= (-\beta_2 \sum_{j=0}^{i-1} f_j) D^4 + (1 - \beta_1 (\sum_{j=0}^{i-1} f_j)^2 + 2\beta_2 \sum_{j=0}^{i-1} f_j') D^3 + ((1 + M\beta_1) \sum_{j=0}^{i-1} f_j + 2\beta_1 \sum_{j=0}^{i-1} f_j \sum_{j=0}^{i-1} f_j' - 2\beta_2 \sum_{j=0}^{i-1} f_j'') D^2 + \\ &+ (2\beta_1 \sum_{j=0}^{i-1} f_j \sum_{j=0}^{i-1} f_j'' - 2 \sum_{j=0}^{i-1} f_j' + 2\beta_2 \sum_{j=0}^{i-1} f_j''' - \lambda - M) D + ((1 + M\beta_1) \sum_{j=0}^{i-1} f_j'' + 2\beta_1 \sum_{j=0}^{i-1} f_j' \sum_{j=0}^{i-1} f_j''' - 2\beta_1 \sum_{j=0}^{i-1} f_j \sum_{j=0}^{i-1} f_j'' - \beta_2 \sum_{j=0}^{i-1} f_j^{iv}), \\ A_{22} &= (1 + \frac{4}{3}R) D^2 + Pr (\sum_{j=0}^{i-1} f_j) D - Pr (\sum_{j=0}^{i-1} f_j'), \\ A_{21} &= 2 Pr Ec \left( \sum_{j=0}^{i-1} f_j'' \right) D^2 + \left( 2MPPrEc \sum_{j=0}^{i-1} f_j' - Pr \sum_{j=0}^{i-1} \theta_j \right) D + Pr \left( \sum_{j=0}^{i-1} \theta_j' \right) \\ A_{33} &= D^2 + Sc (\sum_{j=0}^{i-1} f_j - \tau \sum_{j=0}^{i-1} \theta_j') D + (K_2 - Sc \sum_{j=0}^{i-1} f_j' - Sc \tau \sum_{j=0}^{i-1} \theta_j'') \\ A_{31} &= -Sc (\sum_{j=0}^{i-1} \phi_j) D + Sc (\sum_{j=0}^{i-1} \phi_j') \\ A_{32} &= -Sc \tau \left( \sum_{j=0}^{i-1} \phi_j \right) D^2 - Sc \tau \left( \sum_{j=0}^{i-1} \phi_j' \right) D \\ A_{12} &= \gamma, \quad A_{13} = N\gamma, \quad A_{23} = 0. \end{aligned}$$

The resultant system of Eq. 24 is readily solved as:

$$X_i = A_{i-1}^{-1} R_{i-1}. \tag{25}$$

#### 4. Convergence analysis

The convergence of series solutions to the momentum, temperature, and concentration equations is shown in Table 1. Table 1 clearly shows that a few orders of the SLM series, starting from the third iteration and delivering accuracy up to nine decimal places, are in great agreement with the findings obtained by SLM.

#### 5. Numerical scheme testing

Here, we test the validity of our numerical results and contrast them with those of published works as

limiting examples. So, we contrast the outcomes of this study with those found in the literature (Ghadikolaie et al., 2018; Salah and Elhafian, 2019; Noor, 2012; Shateyi, 2013). It is found that our results are in excellent agreement with Noor (2012) and Shateyi (2013) as shown in Tables 2-5.

#### 6. Results and discussion

The outcomes of the successive linearization method are presented in this section. The local skin friction coefficient, the local Nusselt number, and the local Sherwood number are reported for various values of the physical parameters significant in this study based on the numerical computations shown in Table 5. The dimensionless velocity, temperature, and concentration for various values of the magnetic field parameter  $M$  are shown, accordingly, in Fig. 1.

**Table 1:** Convergence of SLM solutions with respect to several orders of approximations when  $Pr = 0.7, R = 0.3, Sc = Ec = 0.5; B_1 = \tau = 0.2, B_2 = 0.01, M = K_2 = \lambda = \gamma = N = 1$

Order of approximation	$-f''(0)$	$-\theta'(0)$	$-\phi'(0)$
1	1.015899184	0.526023196	1.270002402
2	1.016473962	0.526877992	1.269425856
3	1.016474784	0.526880803	1.269425842
4	1.016474783	0.526880805	1.269425843
5	1.016474783	0.526880805	1.269425843
10	1.016474783	0.526880805	1.269425843
20	1.016474783	0.526880805	1.269425843
30	1.016474783	0.526880805	1.269425843
40	1.016474783	0.526880805	1.269425843
50	1.016474783	0.526880805	1.269425843

**Table 2:** Comparison of the SLM findings of  $-f''(0), -\theta'(0)$  and  $-\phi'(0)$  with those found in Noor (2012) and Shateyi (2013) for various magnetic parameter values

M	$-f''(0)$			$-\theta'(0)$			$-\phi'(0)$		
	(Noor, 2012)	(Shateyi, 2013)	Present	(Noor, 2012)	(Shateyi, 2013)	Present	(Noor, 2012)	(Shateyi, 2013)	Present
0.0	0.611105	0.611105243	0.611105243	0.63589	0.63588754	0.63588754	1.30284	1.30284353	1.30284355
0.5	0.81242	0.81241682	0.81241680	0.53469	0.53469349	0.53469349	1.28395	1.28395421	1.28395421
1.0	0.99660	0.99658887	0.99658887	0.44624	0.44621677	0.44621678	1.26728	1.26727829	1.26727829
2.0	1.38934	1.32487675	1.32487676	0.28290	0.28719193	0.29719196	1.24527	1.23899430	1.23899343

**Table 3:** Comparison of the SLM findings of  $-f''(0), -\theta'(0)$  and  $-\phi'(0)$  with those found in Noor (2012) and Shateyi (2013) for various chemical reaction parameter values

$K_2$	$-f''(0)$			$-\theta'(0)$			$-\phi'(0)$		
	(Noor, 2012)	(Shateyi, 2013)	Present	(Noor, 2012)	(Shateyi, 2013)	Present	(Noor, 2012)	(Shateyi, 2013)	Present
0.0	0.92029	0.92027899	0.92027900	0.47847	0.47854048	0.47854048	0.70970	0.70959986	0.70959986
0.5	0.96935	0.96934259	0.96934259	0.45647	0.45644780	0.45644781	1.03512	1.03512125	1.03512125
1.0	0.99660	0.99658887	0.99658887	0.44624	0.44621677	0.44621678	1.26728	1.26727829	1.26727829
2.0	1.03073	1.03072331	1.03072331	0.43520	0.43517486	0.43517487	1.62744	1.62744240	1.62744240

**Table 4:** Comparison of SLM finding of  $f(\eta)$  with those found in Ghadikolaei et al. (2018) and Salah and Elhafian (2019) for various values of  $\eta$  when  $M = \beta_1 = \lambda = 0.0$  and  $\beta_2 = 0.01$

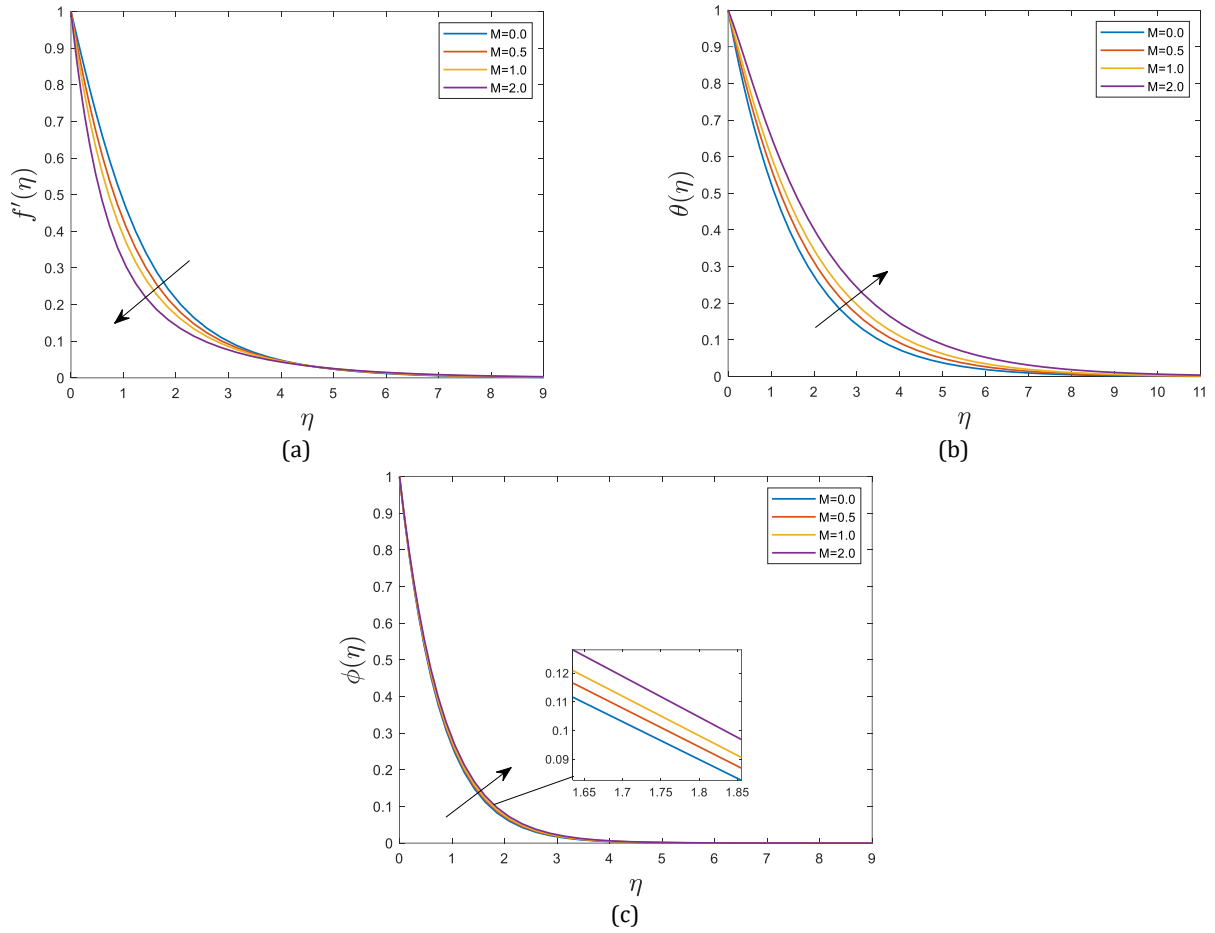
$\beta_2$	$\eta$	(Ghadikolaei et al., 2018)	(Salah and Elhafian, 2019)	Present
0.01	0	0	0	0
	0.1	0.095199	0.095194	0.095186
	0.2	0.181400	0.181338	0.181357
	0.5	0.394050	0.393892	0.393919
	1	0.633463	0.633460	0.633440
	2	0.866679	0.867642	0.867634
	3	0.952228	0.954211	0.954216
	4	0.983566	0.986229	0.986225
	5	-	0.998059	0.998057

Fig. 1a shows that when the magnetic parameter  $M$  increases, the velocity profiles decrease. The Lorentz force, which opposes the flow, is produced physically by increasing the magnetic field intensity normal to the flow in an electrically conducting fluid. Delaying the transition from laminar to turbulent flow is therefore possible by applying a mild magnetic field to the flow. Figs. 1b and 1c show how the heat and concentration profiles increase as a result of a reduction in flow velocity brought on by an increase in magnetic field intensity. In terms of physics, creating a magnetic field heats the fluid, which minimizes heat and mass transfers from the wall and raises the fluid temperature and concentration distributions. We show how the permeability of the medium affects the flow velocity, temperature, and concentration in Fig. 2, accordingly. As the values of the porosity parameter

are raised, we notice that the dimensionless velocity drops. Physically, as shown in Figs. 2b and 2c, porosity causes more fluid to be removed from the boundary layer, which reduces the velocity boundary layer but raises the thermal and solutal boundary layers. The impact of a chemical reaction on the fluid velocity and concentration profiles is depicted in Fig. 3. In this study, we examine the results of a chemical reaction that is destructive ( $K_2 > 0$ ). When the chemical reaction increases, it is observed that both velocity and concentration distributions decrease. Chemical reactions in destructive cases physically occur with numerous disturbances. High molecular mobility is therefore brought on by this, increasing the transport phenomena and lowering the concentration distributions in the fluid flow.

**Table 5:** Different values of skin friction coefficient, local Nusselt number, and local Sherwood number using SLM for different parameters

$M$	$Pr$	$Sc$	$Ec$	$\tau$	$R$	$\beta_1$	$\beta_2$	$\lambda$	$K_2$	$-f''(0)$	$-\theta'(0)$	$-\phi'(0)$	
0.0	0.7	0.5	0.5	0.2	0.3	0.2	0.01	1	1	0.609947046	0.636445163	1.303014577	
0.5										0.809881616	0.535280287	1.284165328	
1	0.5	0.7	1	2	0.0	0.5	1	2	0.0	0.992898218	0.446813554	1.267516387	
2										1.319413986	0.297779647	1.239261478	
0.5										0.972400832	0.380094847	1.266122992	
0.7										0.992898218	0.446813554	1.267516387	
1										1.016474783	0.526880805	1.269425843	
2										1.065420133	0.705817782	1.274594135	
0.0										0.960370583	0.459290077	1.000000000	
0.5										0.992898218	0.446813554	1.267516387	
1										1.018513539	0.438066037	1.509998780	
2										1.056076046	0.427095037	1.939824715	
0.0	0.5	1	2	0.0	0.5	0.0	0.01	1	0.0	1.016399546	0.640108398	1.280537658	
										0.5	0.992898218	0.446813554	1.267516387
										2	1.018513539	0.438066037	1.509998780
										0.0	1.056076046	0.427095037	1.939824715
										0.5	0.992898218	0.446813554	1.267516387
										2	0.919976327	-0.117554638	1.230756511
										0.0	0.868009849	-0.486173378	1.207998592
										0.2	0.990253256	0.447659907	1.242019127
										1	0.992898218	0.446813554	1.267516387
										2	1.003259304	0.443559447	1.371633438
0.0	0.3	1	2	0.0	0.3	0.0	0.01	1	0.0	1.015708041	0.439782694	1.506363067	
										0.3	1.015096607	0.522098484	1.269304699
										1	0.992898218	0.446813554	1.267516387
										2	0.962535424	0.348907815	1.265536154
										0.0	0.939473855	0.278314048	1.264369955
										0.2	0.946737992	0.460960811	1.272433121
										0.5	0.992898218	0.446813554	1.267516387
										0.7	1.062647573	0.426458080	1.260452328
										0.0	1.109107790	0.413527999	1.255976908
										0.0	1.005663188	0.443350315	1.358033239
0.0	0.01	0.02	0.03	0.0	0.0	0.0	0.01	0.02	0.03	1.001983519	0.443954786	1.358436203	
										0.998352682	0.444554934	1.358836087	
										0.994769168	0.445150843	1.359232957	
										0.611558666	0.506969158	1.293013786	
										0.811605985	0.477045411	1.279575541	
										0.992898218	0.446813554	1.267516387	
										1.312896499	0.388145096	1.246753000	
										0.916446055	0.479043487	0.710066972	
										0.965620269	0.457013247	1.035419418	
										0.992898218	0.446813554	1.267516387	
2	1.027038431	0.435809893	1.627625067										



**Fig. 1:** Effect of the magnetic field  $M$  on a) velocity, b) temperature, and c) concentration

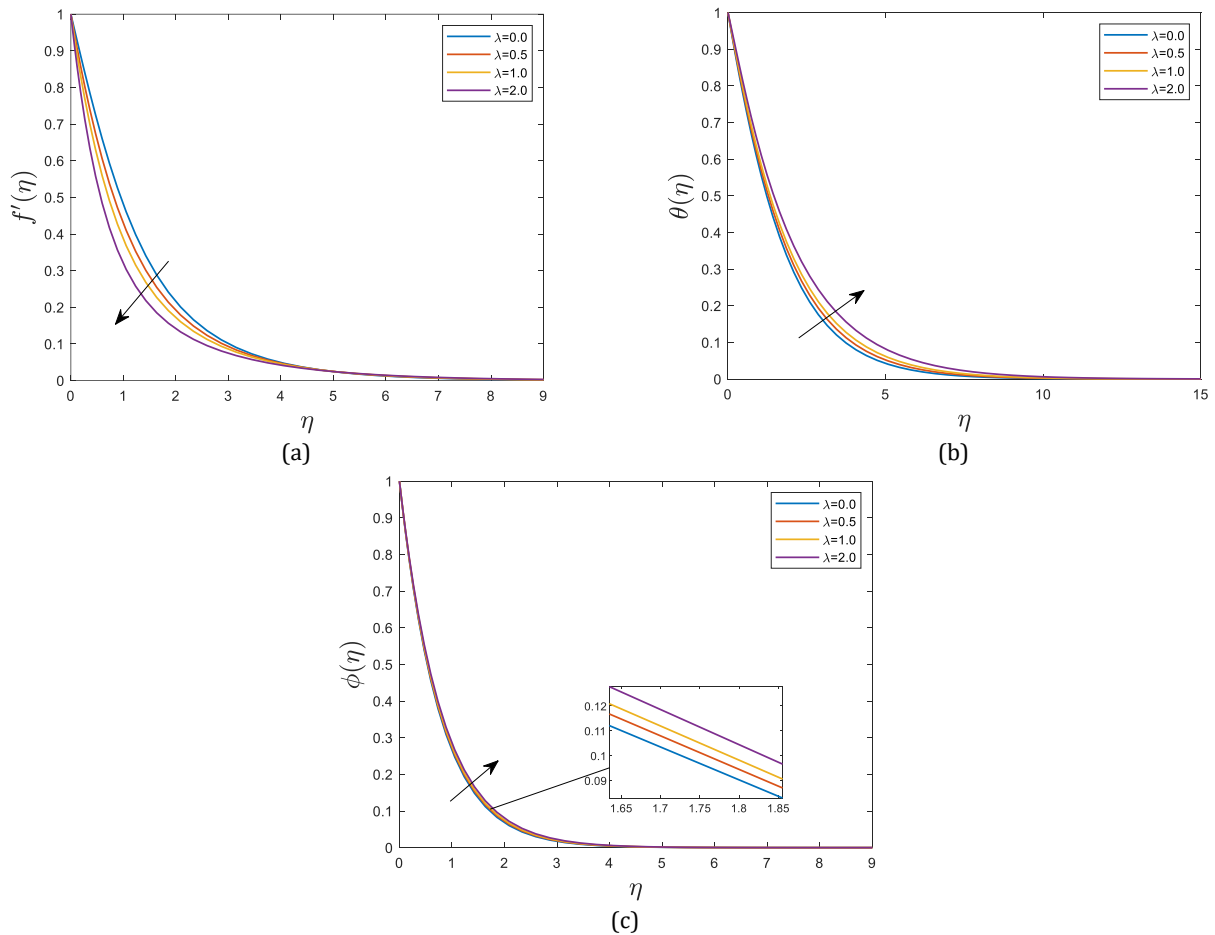


**Fig. 2:** Effect of the porosity parameter  $\lambda$  on a) velocity, b) temperature, and c) concentration

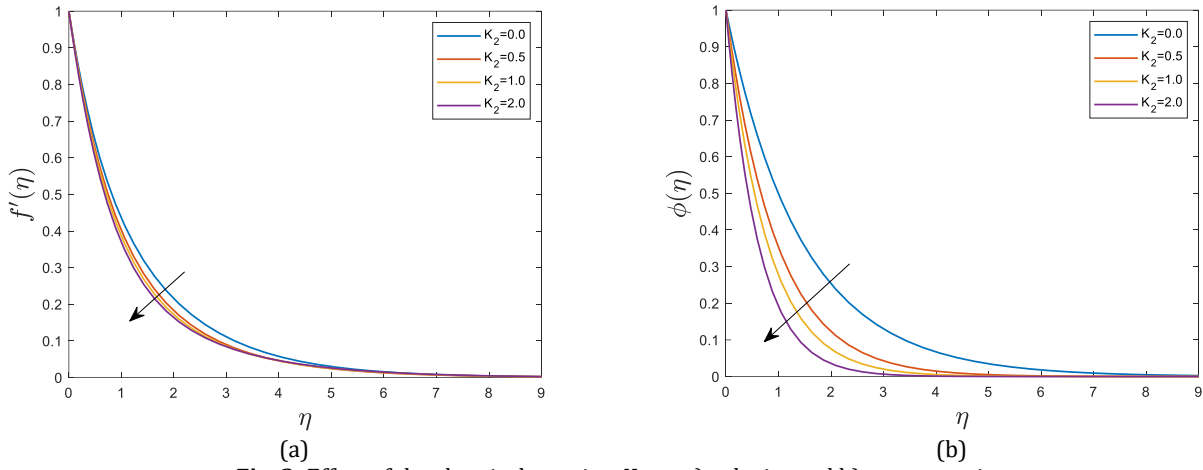


Fig. 3: Effect of the chemical reaction  $K_2$  on a) velocity and b) concentration

Fig. 4, respectively, shows the impacts of the Deborah number  $\beta_1$  on the velocity and temperature curves. As the temperature rises, we see that the boundary layer thickness decreases with rising values of  $\beta_1$ . The Deborah number, in terms of physics, is the ratio between the relaxation time, which describes how long a material needs to respond to pressures or deformations, and the typical time scale of an experiment exploring the response of the material. Higher Deborah numbers result in a material's behavior that is increasingly dominated by elasticity and behaves solidly, decreasing the flow velocity and raising the fluid's temperature.

Fig. 5 shows accordingly how thermal radiation affects fluid velocity and temperature. It has been noted that thermal radiation increases the boundary layer's fluid velocity. It's noteworthy to notice that the distribution of temperature inside the fluid is significantly influenced by thermal radiation. As the heat radiation increases, the fluid temperature rises, as seen in Fig. 5b. This is a result of the fact that rising thermal radiation parameter values imply rising boundary layer radiation, which raises the thermal boundary layer temperature profile values.

The fluctuation of the temperature and velocity distributions in the boundary layer for different

Eckert number  $Ec$  values are shown in Fig. 6. We see that the boundary layer's velocity distribution is only marginally affected by the Eckert number as it increases. By examining Fig. 6b, we can see that the Eckert number has a significant impact on raising the temperature in the flow region. This is because heat energy from frictional heating is stored in the liquid. Increased fluid temperature is the result of rising  $Ec$ , so to speak.

The effects of the Prandtl number on the velocity and temperature distributions are shown in Fig. 7. As the Prandtl number rises, we notice that the velocity and temperature profiles both become smaller. This is due to the fact that as  $Pr$  rises, thermal diffusivity declines, decreasing the thermal boundary layer's capacity to transport energy.

Fig. 8 illustrates the impacts of the thermophoretic parameter  $\tau$  and the Schmidt number  $Sc$ , respectively. We notice that as the thermophoretic parameter  $\tau$  is increased, the particle concentration decreases across the flow region. We notice that the effect of increasing the thermophoretic parameter  $\tau$  is restricted to significantly increasing the wall slope of the concentration profiles while lowering the concentration.

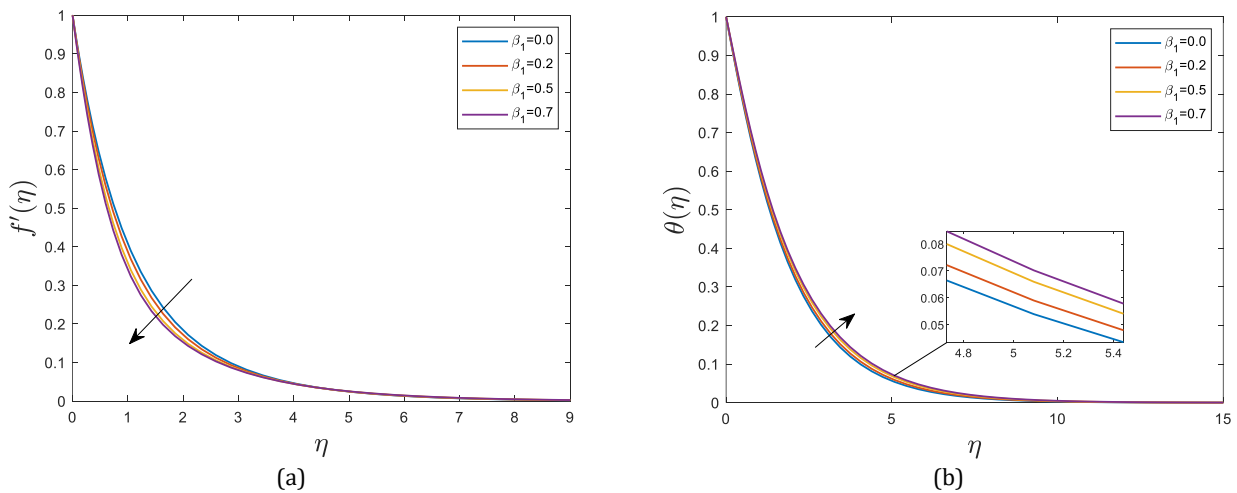
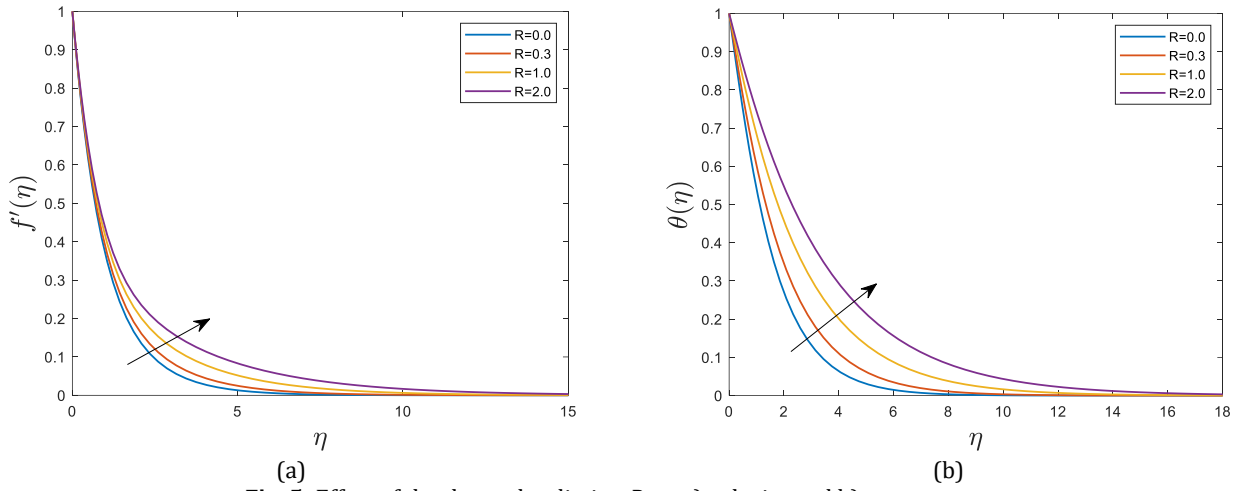
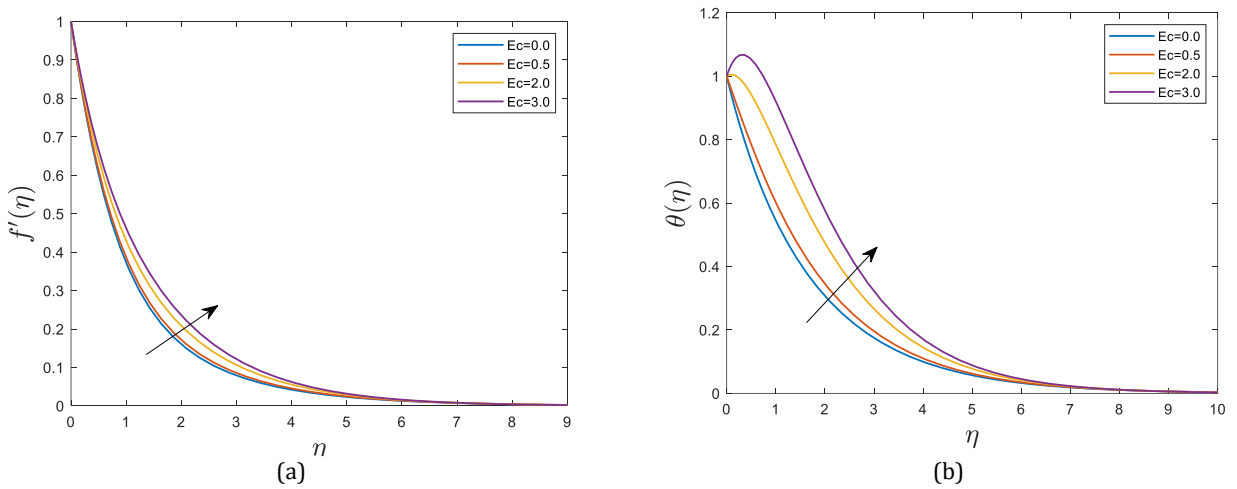


Fig. 4: Effect of the Deborah number  $\beta_1$  on a) velocity and b) temperature



**Fig. 5:** Effect of the thermal radiation  $R$  on a) velocity and b) temperature



**Fig. 6:** Effect of the Eckert number  $Ec$  on a) velocity and b) temperature

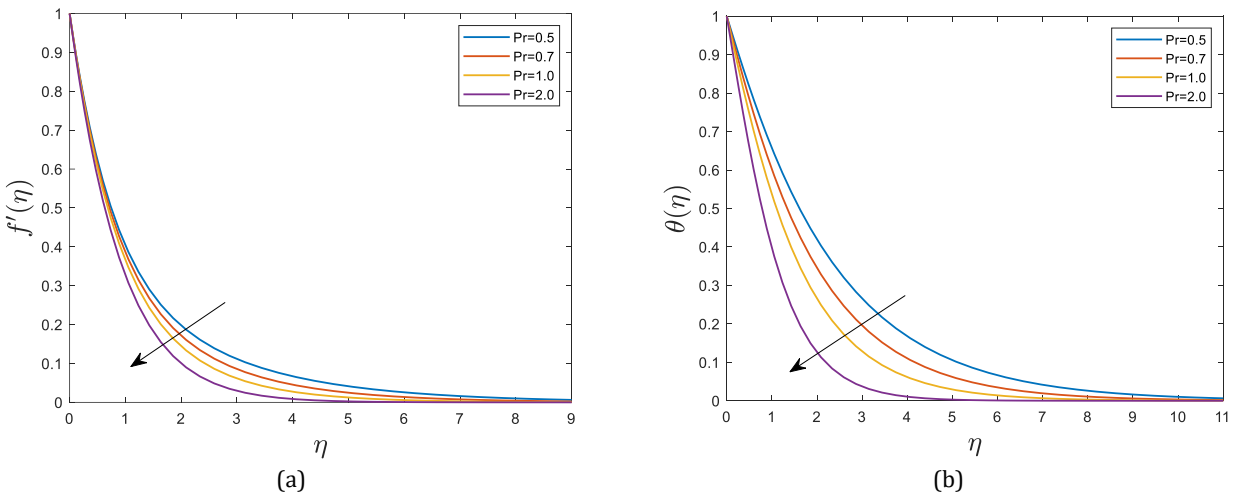


**Fig. 7:** Effect of the Prandtl number  $Pr$  on a) velocity and b) temperature

The Schmidt number  $Sc$  describes how effective species diffusion in the concentration boundary layer is compared to momentum transport diffusion in the hydrodynamic boundary layer. This graph makes it quite evident that as the Schmidt number  $Sc$  rises, the concentration boundary layer width decreases. This effect happens as a result of the concentration of species becoming heavier as  $Sc$  increases.

Finally, Fig. 9 illustrates how  $\beta_2$  affects the velocity and temperature profiles. It should be noted

that as  $\beta_2$  is increased, the influence is found to be extremely minimal for both aspects. Additionally, by setting  $\beta_1 = 0$ ,  $\beta_2 = 0$ , and  $\beta_1 = \beta_2 = 0$ , the second-grade, Maxwell, and viscous cases are recovered, respectively.

**7. Conclusion**

The magnetohydrodynamic flow of an Oldroyd-B fluid across a vertical stretching sheet in a Darcian porous medium under the impact of thermophoresis,

heat radiation, and a homogeneous chemical reaction has been solved using SLM. The analysis found that this strategy might potentially be applied to even the most challenging non-linear issues. Thermal radiation, porosity, Deborah number, and magnetic strength were all found to have a significant impact on velocity profiles. The temperature of the fluid was shown to rise with increasing magnetic force, porosity, Deborah

number, thermal radiation, and Eckert number but to fall with increasing Prandtl number. As it has increased, the influence is found to be extremely minimal for both aspects. The existence of a chemical reaction and thermophoresis were both found to have a considerable impact on the fluid concentration profiles. In future work, we can modify the problem to three-dimensional coordinates with a heat sink.

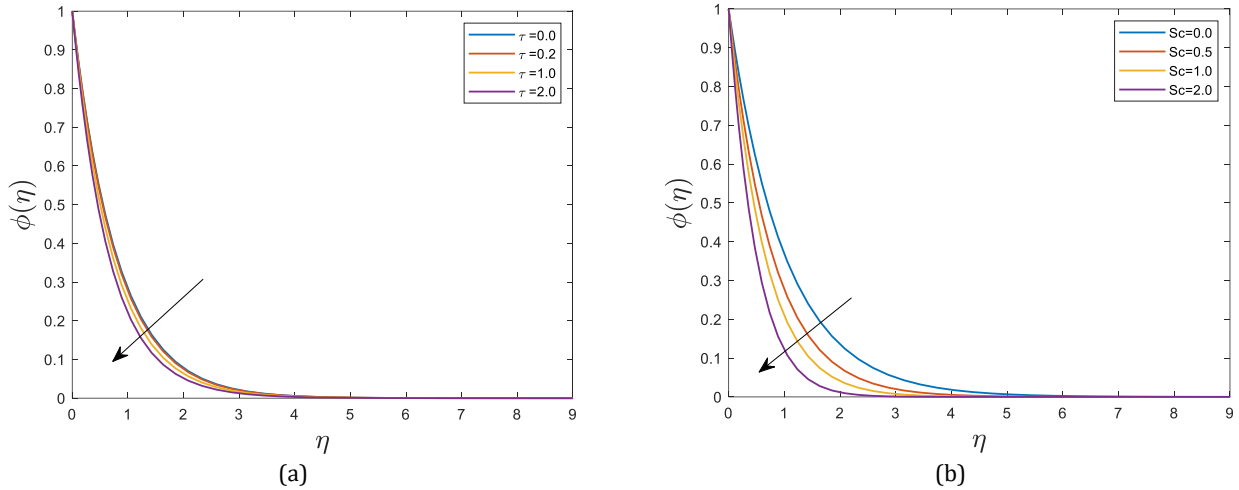


Fig. 8: Effects of the thermophoretic parameter a)  $\tau$  and b)  $Sc$  on concentration

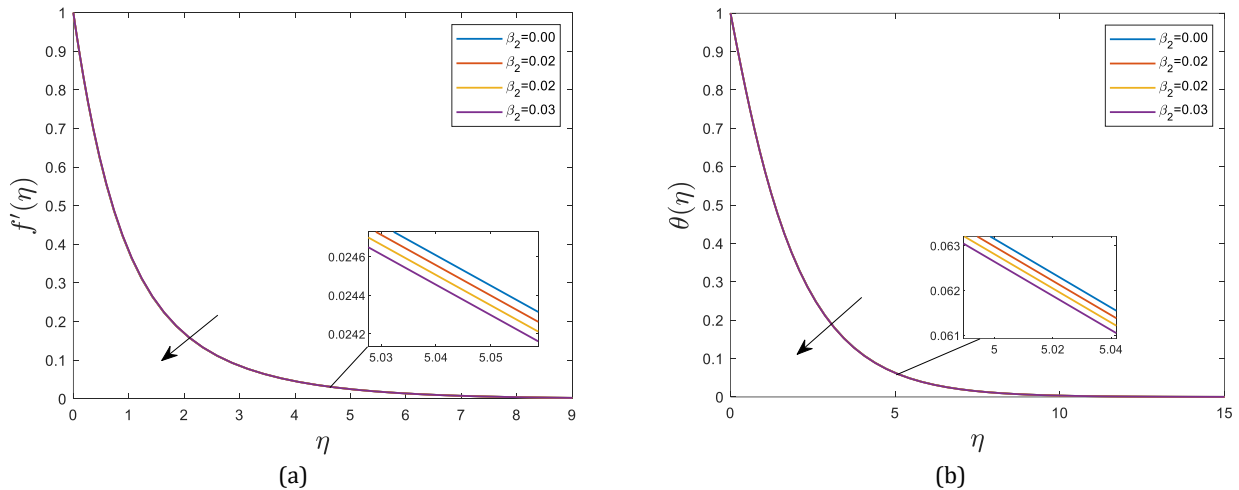


Fig. 9: Effects of Deborah number  $\beta_2$  on a) velocity and b) temperature

**List of symbols**

$(x, y)$	Cartesian coordinates [m]	$D$	Molecular diffusivity
$(u, v)$	Velocity components [ms <sup>-1</sup> ]	$V_T$	Thermophoretic velocity
$\nu$	Kinematic viscosity [m <sup>2</sup> s <sup>-1</sup> ]	$K_2$	Chemical reaction
$\mu$	Dynamic viscosity [kg m <sup>-1</sup> s <sup>-1</sup> ]	$\tau$	A thermophoretic parameter
$\beta_1$	Relaxation time [s]	$\gamma$	local buoyancy parameter
$\beta_2$	Retardation time [s]	$M$	Hartman number
$\rho$	Density of fluid [Kg m <sup>-3</sup> ]	$\lambda$	porosity parameter
$\sigma$	The electric conductivity [Sm <sup>-1</sup> ]	$R$	Radiation parameter
$B_0$	Magnetic fluid [Wbm <sup>-2</sup> ]	$Pr$	Prandtl number
$g$	Gravitational acceleration [ms <sup>-2</sup> ]	$Ec$	Eckert number
$C$	Fluid concentration	$Sc$	Schmidt number
$T$	Fluid temperature [K]	$C_w$	Concentration field at the surface [mol]
$\beta_T$	Coefficient of thermal expansion	$C$	Concentration of field [mol]
$\beta_C$	Coefficient of concentration expansion	$C_\infty$	Ambient concentration field [mol]
$\lambda_g$	Fluid thermal conductivity [Wm <sup>-1</sup> K <sup>-1</sup> ]	$U_w$	Velocity at the wall [ ms <sup>-1</sup> ]
$c_p$	Specific heat [JK <sup>-1</sup> m <sup>-3</sup> ]	$T_w$	Surface temperature [K]
$q_r$	Radiative heat flux	$T_\infty$	Ambient temperature [K]

## Compliance with ethical standards

## Conflict of interest

The author(s) declared no potential conflicts of interest with respect to the research, authorship, and/or publication of this article.

## References

- Ahmed MAM, Mohammed ME, and Khidir AA (2015). On linearization method to MHD boundary layer convective heat transfer with low pressure gradient. *Propulsion and Power Research*, 4(2): 105-113.  
<https://doi.org/10.1016/j.jprr.2015.04.001>
- Ahmed MAM, Mohammed ME, and Khidir AA (2016). The effects of cross-diffusion and radiation on mixed convection from a vertical flat plate embedded in a fluid-saturated porous medium in the presence of viscous dissipation. *Propulsion and Power Research*, 5(2): 149-163.  
<https://doi.org/10.1016/j.jprr.2016.05.001>
- Azeem KW, Khan M, and Malik R (2014). Three-dimensional flow of an Oldroyd-B nanofluid towards stretching surface with heat generation/absorption. *PLOS ONE*, 9(8): e105107.  
<https://doi.org/10.1371/journal.pone.0105107>  
**PMid:25170945** **PMCID:PMC4149422**
- Cortell R. (2006). A note on flow and heat transfer of a viscoelastic fluid over a stretching sheet. *International Journal of Non-Linear Mechanics*, 41(1): 78-85.  
<https://doi.org/10.1016/j.ijnonlinmec.2005.04.008>
- Daoud Y, Abdalbagi M, and Khidir AA (2021). On the solution of magneto-hydrodynamics three-dimensional flow due to a stretching sheet in a porous medium using the successive linearization method. *Chinese Journal of Physics*, 73: 232-238.  
<https://doi.org/10.1016/j.cjph.2021.06.011>
- Ghadikolaei SS, Hosseinzadeh K, Yassari M, Sadeghi H, and Ganji DD (2018). Analytical and numerical solution of non-Newtonian second-grade fluid flow on a stretching sheet. *Thermal Science and Engineering Progress*, 5: 309-316.  
<https://doi.org/10.1016/j.tsep.2017.12.010>
- Gireesha BJ, Kumar KG, Ramesh GK, and Prasannakumara BC (2018). Nonlinear convective heat and mass transfer of Oldroyd-B nanofluid over a stretching sheet in the presence of uniform heat source/sink. *Results in Physics*, 9: 1555-1563.  
<https://doi.org/10.1016/j.rinp.2018.04.006>
- Hayat T, Imtiaz M, Alsaedi A, and Almezal S (2016). On Cattaneo-Christov heat flux in MHD flow of Oldroyd-B fluid with homogeneous-heterogeneous reactions. *Journal of Magnetism and Magnetic Materials*, 401: 296-303.  
<https://doi.org/10.1016/j.jmmm.2015.10.039>
- Hayat T, Muhammad T, Shehzad SA, and Alsaedi A (2015). Temperature and concentration stratification effects in mixed convection flow of an Oldroyd-B fluid with thermal radiation and chemical reaction. *PLOS ONE*, 10(6): e0127646.  
<https://doi.org/10.1371/journal.pone.0127646>  
**PMid:26102200** **PMCID:PMC4478041**
- Hayat T, Shehzad SA, Al-Mezel S, and Alsaedi A (2014). Three-dimensional flow of an Oldroyd-B fluid over a bidirectional stretching surface with prescribed surface temperature and prescribed surface heat flux. *Journal of Hydrology and Hydromechanics*, 62(2): 117-125.  
<https://doi.org/10.2478/johh-2014-0016>
- Hayat T, Shehzad SA, Alsaedi A, and Alhothuali MS (2013). Three-dimensional flow of Oldroyd-B fluid over surface with convective boundary conditions. *Applied Mathematics and Mechanics*, 34(4): 489-500.  
<https://doi.org/10.1007/s10483-013-1685-9>
- Hussaini MY and Zang TA (1987). Spectral methods in fluid dynamics. *Annual Review of Fluid Mechanics*, 19(1): 339-367.  
<https://doi.org/10.1146/annurev.fl.19.010187.002011>
- Khan M, Yasir M, Alshomrani AS, Sivasankaran S, Aladwani YR, and Ahmed A (2022). Variable heat source in stagnation-point unsteady flow of magnetized Oldroyd-B fluid with cubic autocatalysis chemical reaction. *Ain Shams Engineering Journal*, 13(3): 101610.  
<https://doi.org/10.1016/j.asej.2021.10.005>
- Khidir AA (2023). Application of successive linearisation method on mixed convection boundary layer flow of nanofluid from an exponentially stretching surface with magnetic field effect. *Journal of Nanofluids*, 12(2): 465-475.  
<https://doi.org/10.1166/jon.2023.1961>
- Liao S (2003). *Beyond perturbation: Introduction to the homotopy analysis method*. CRC Press, Boca Raton, USA.
- Mabood F, Bognár G, and Shafiq A (2020). Impact of heat generation/absorption of magnetohydrodynamics Oldroyd-B fluid impinging on an inclined stretching sheet with radiation. *Scientific Reports*, 10: 17688.  
<https://doi.org/10.1038/s41598-020-74787-2>  
**PMid:33077753** **PMCID:PMC7572406**
- Makinde OD (2008). Effect of arbitrary magnetic Reynolds number on MHD flows in convergent-divergent channels. *International Journal of Numerical Methods for Heat and Fluid Flow*, 18(6): 697-707.  
<https://doi.org/10.1108/09615530810885524>
- Makukula Z, Motsa SS, and Sibanda P (2010a). On a new solution for the viscoelastic squeezing flow between two parallel plates. *Journal of Advanced Research in Applied Mathematics*, 2(4): 31-38. <https://doi.org/10.5373/jaram.455.060310>
- Makukula ZG, Sibanda P, and Motsa SS (2010b). A novel numerical technique for two-dimensional laminar flow between two moving porous walls. *Mathematical Problems in Engineering*, 2010: 528956. <https://doi.org/10.1155/2010/528956>
- Motsa SS, Makukula ZG, and Shateyi S (2015). Numerical investigation of the effect of unsteadiness on three-dimensional flow of an Oldroyd-B fluid. *PLOS ONE*, 10(7): e0133507.  
<https://doi.org/10.1371/journal.pone.0133507>  
**PMid:26196291** **PMCID:PMC4510369**
- Narayana M and Sibanda P (2012). On the solution of double-diffusive convective flow due to a cone by a linearization method. *Journal of Applied Mathematics*, 2012: 587357.  
<https://doi.org/10.1155/2012/587357>
- Noor NFM (2012). Analysis for MHD flow of a Maxwell fluid past a vertical stretching sheet in the presence of thermophoresis and chemical reaction. *World Academy of Science, Engineering and Technology*, 64: 1019-1023.
- Paul A and Das TK (2023). Thermal and mass transfer aspects of MHD flow across an exponentially stretched sheet with chemical reaction. *International Journal of Ambient Energy*, 44(1): 1563-1574.  
<https://doi.org/10.1080/01430750.2023.2179110>
- Pires M and Sequeira A (2011). Flows of generalized Oldroyd-B fluids in curved pipes. In: Escher J, Guidotti P, Hieber M, and Zajaczkowski W (Eds.), *Parabolic problems: The Herbert Amann festschrift*: 21-43. Volume 80, Springer, Basel, Switzerland. [https://doi.org/10.1007/978-3-0348-0075-4\\_2](https://doi.org/10.1007/978-3-0348-0075-4_2)
- Raptis A (1998). Flow of a micropolar fluid past a continuously moving plate by the presence of radiation. *International Journal of Heat and Mass Transfer*, 18(41): 2865-2866.  
[https://doi.org/10.1016/S0017-9310\(98\)00006-4](https://doi.org/10.1016/S0017-9310(98)00006-4)
- Reddy NN, Rao VS, and Reddy BR (2021). Chemical reaction impact on MHD natural convection flow through porous medium past an exponentially stretching sheet in presence of heat source/sink and viscous dissipation. *Case Studies in Thermal Engineering*, 25: 100879.  
<https://doi.org/10.1016/j.csite.2021.100879>

- Rubbab Q, Husnine SM, and Mahmood AMIR (2009). Exact solutions of generalized Oldroyd-B fluid subject to a time-dependent shear stress in a pipe. *Journal of Prime Research in Mathematics*, 5: 139-148.
- Sajid M, Abbas Z, Javed T, and Ali N (2010). Boundary layer flow of an Oldroyd-B fluid in the region of a stagnation point over a stretching sheet. *Canadian Journal of Physics*, 88(9): 635-640. <https://doi.org/10.1139/P10-049>
- Salah F (2022). Chemical reaction and generalized heat flux model for Powell-Eyring model with radiation effects. *International Journal of Mathematics and Mathematical Sciences*, 2022: 4076426. <https://doi.org/10.1155/2022/4076426>
- Salah F and Elhafian MH (2019). Numerical solution for heat transfer of non-Newtonian second-grade fluid flow over stretching sheet via successive linearization method. *IAENG International Journal of Applied Mathematics*, 49(4): 505-512.
- Salah F and Sidahmed AO (2022). Chemical reaction and radiation effects on MHD flow of Oldroyd-B fluid through porous medium past an exponentially stretching sheet with heat sink. *Journal of Applied Mathematics*, 2022: 6582295. <https://doi.org/10.1155/2022/6582295>
- Salah F, Alzahrani A, Sidahmed AO, and Viswanathan KK (2019). A note on thin-film flow of Eyring-Powell fluid on the vertically moving belt using successive linearization method. *International Journal of Advanced and Applied Sciences*, 6(2): 17-22. <https://doi.org/10.21833/ijaas.2019.02.004>
- Salah F, Sidahmed AO, and Viswanathan KK (2023). Chemical MHD Hiemenz flow over a nonlinear stretching sheet and Brownian motion effects of nanoparticles through a porous medium with radiation effect. *Mathematical and Computational Applications*, 28(1): 21. <https://doi.org/10.3390/mca28010021>
- Seini YI and Makinde OD (2013). MHD boundary layer flow due to exponential stretching surface with radiation and chemical reaction. *Mathematical Problems in Engineering*, 2013: 163614. <https://doi.org/10.1155/2013/163614>
- Shankaralingappa BM, Prasannakumara BC, Giresha BJ, and Sarris IE (2021). The impact of Cattaneo-Christov double diffusion on Oldroyd-B Fluid flow over a stretching sheet with thermophoretic particle deposition and relaxation chemical reaction. *Inventions*, 6(4): 95. <https://doi.org/10.3390/inventions6040095>
- Shateyi S (2013). A new numerical approach to MHD flow of a Maxwell fluid past a vertical stretching sheet in the presence of thermophoresis and chemical reaction. *Boundary Value Problems*, 2013: 196. <https://doi.org/10.1186/1687-2770-2013-196>
- Shateyi S and Motsa SS (2010). Variable viscosity on magnetohydrodynamic fluid flow and heat transfer over an unsteady stretching surface with Hall effect. *Boundary Value Problems*, 2010: 257568. <https://doi.org/10.1155/2010/257568>
- Sidahmed A and Salah F (2022). Radiation effects on MHD flow of second grade fluid through porous medium past an exponentially stretching sheet with chemical reaction. *Journal of Advanced Research in Fluid Mechanics and Thermal Sciences*, 99(2): 1-16. <https://doi.org/10.37934/arfmts.99.2.116>
- Waqas M, Hayat T, Shehzad SA, and Alsaedi A (2018). Transport of magnetohydrodynamic nanomaterial in a stratified medium considering gyrotactic microorganisms. *Physica B: Condensed Matter*, 529: 33-40. <https://doi.org/10.1016/j.physb.2017.09.128>
- Yasir M and Khan M (2023). Dynamics of unsteady axisymmetric of Oldroyd-B material with homogeneous-heterogeneous reactions subject to Cattaneo-Christov heat transfer. *Alexandria Engineering Journal*, 74: 665-674. <https://doi.org/10.1016/j.aej.2023.05.065>
- Yasir M, Ahmed A, Khan M, Alzahrani AK, Malik ZU, and Alshehri AM (2023). Mathematical modelling of unsteady Oldroyd-B fluid flow due to stretchable cylindrical surface with energy transport. *Ain Shams Engineering Journal*, 14(1): 101825. <https://doi.org/10.1016/j.asej.2022.101825>
- Yasir M, Ahmed A, Khan M, and Ullah MZ (2021). Convective transport of thermal and solutal energy in unsteady MHD Oldroyd-B nanofluid flow. *Physica Scripta*, 96(12): 125266. <https://doi.org/10.1088/1402-4896/ac3b67>